American Mineralogist, Volume 80, pages 1116–1131, 1995

Complex polytypism: Relationships between serpentine structural characteristics and deformation

Jillian F. Banfield, Sturges W. Bailey,† William W. Barker
Department of Geology and Geophysics, University of Wisconsin–Madison, 1215 West Dayton Street, Madison, Wisconsin 53706, U.S.A.

Robert C. Smith II
Bureau of Topographic and Geologic Survey, Department of Environmental Resources, Harrisburg, Pennsylvania 17105-8453, U.S.A.

Abstract

Serpentinite from Woods Chrome Mine, Lancaster County, Pennsylvania, consists of planar serpentine, randomly interstratified serpentine-chlorite, a series of phases based on regular interstratification of serpentine and chlorite, minor chlorite, polygonal serpentine, and antigorite. The serpentine mineralogy is complex, including structures with long-range order in (1) the octahedral cation sequence and (2) the sequence of displacements between adjacent 1:1 layers. In addition to previously described (but generally less common) $2T$, $2H_1$, $2H_2$, $6R_1$, and $6R_2$ lizardite polytypes, the assemblage contains planar serpentines with long-range order in octahedral cation sequences but with random **b**/3 (and possibly **a**/3) displacements between adjacent layers. By comparison with calculated electron diffraction intensities, we identified three- (I,I,II), four- (I,I,II,II and I,I,I,II), five- (I,II,I,II,II), six- (II,I,I,I,II,II), seven- (I,II,I,II,II,II,II and I,II,I,II,I,II,II), and nine-layer octahedral sequences. In addition, the assemblage includes rare three- and four-layer serpentines with regular stacking; in some cases the stacking is nonstandard, insofar as zero and $\pm$**b**/3 displacements occur together. By comparison between electron diffraction intensities and calculated patterns, we identified a three-layer regular stacking sequence that involves 0,0,−**b**/3 displacements between adjacent layers ($\alpha = 98°$, $\beta = 90°$, $\gamma = 90°$), a four-layer monoclinic sequence with 0,−**b**/3,0,+**b**/3 ($\alpha = 90°$, $\beta = 90°$, $\gamma = 90°$; I,I,II,II), and three four-layer triclinic sequences with 0,−**b**/3,−**b**/3,−**b**/3 ($\alpha = 90°$, $\beta = 90°$, $\gamma = 90°$), 0,0,0,−**b**/3 ($\alpha = 96°$, $\beta = 90°$, $\gamma = 90°$), and −**b**/3,−**b**/3,−**b**/3,+**b**/3 ($\alpha = 96°$, $\beta = 90°$, $\gamma = 90°$) displacements between adjacent layers. Planar layer silicates exhibit macroscopic preferred orientation. The strong lineation in the foliation defined by the silicate sheets parallels either **a** or **b**, suggesting serpentine crystals were rotated, recrystallized, or both during shear deformation. We suggest that for crystals with **b** parallel to the lineation, deformation induced regular layer displacements. For crystals with **a** parallel to the lineation, periodic displacements of OH planes may have promoted development of regular octahedral cation sequences.

Two-layer (I,II) and three-layer (I,I,II) serpentines and randomly interstratified serpentine-chlorite contain frequent but nonperiodic planar defects perpendicular to **a*** and the pseudo-**a*** axes that are interpreted to displace polytypic sequences. These defects predate chloritization and, in some cases, appear to serve as sites for chlorite nucleation. Layer silicates are crosscut by late-stage polygonized two-layer serpentine with disordered or regular stacking. In some cases with regular stacking, enantiomorphic $6R_2$ segments with a common **c**-axis direction parallel to their boundary are separated by sectors with $2H_2$ stacking. Polygonized serpentines are nucleated on steps at the surfaces of layer silicates and may have developed at a late stage by recrystallization of curved serpentine.

Introduction

Structural and compositional details of layer silicate assemblages may provide insights into the petrogenetic history of the rocks that contain them. Serpentine minerals characterize greenschist facies rocks of ultramafic origin. They are common products of hydrothermal alteration of periodotite, lherzolite, harzburgite, etc., in which primary mafic silicates are converted to assemblages that include chlorite, brucite, lizardite, antigorite, chrysotile, and polygonal serpentine. They form in low-temperature reactions near the Earth's surface. Serpentinization of ultramafic rocks associated with spreading zones

† Deceased November 30, 1994.

0003–004X/95/1112–1116$02.00

profoundly changes their geophysical (magnetic susceptibilities and seismic velocities), isotopic, and chemical characteristics. Serpentine minerals are constituents of chrysotile asbestos, and thus they are also of interest because of concern over their effects on human health.

Although procedures for distinguishing standard polytypes of 1:1 layer silicates, micas, and chlorites are well established (see Bailey, 1988a), the significance of the development of one layer silicate polytype in place of another is poorly understood. In general, factors considered to influence polytype development include (1) the chemistry, temperature, and pressure during growth; (2) crystal-chemical details, including structural distortions of individual layers; and (3) the growth mechanism (particularly if associated with spiral growth on screw dislocations; Baronnet, 1975).

Experimentalists have attempted to define P_{H_2O}-T stability fields for mica polytypes (e.g., Yoder and Eugster, 1955), and observational data have been used to argue that specific polytypes develop in reaction series that correlate with increasing temperature (e.g., type I chlorites are replaced by the II*bb* polytype during metamorphism; see Brown and Bailey, 1962; Karpova, 1969; Curtis et al., 1985; for other discussions on chlorite see Hayes, 1970; Velde, 1965; Walker and Thompson, 1990; Walker, 1993; de Caritat et al., 1993). Other experimental studies on micas suggest that the degree of supersaturation may influence stacking (Amouric and Baronnet, 1983). However, results such as those of Bigi and Brigatti (1994), which reveal numerous complex biotite polytypes in a single assemblage, suggest that factors other than temperature, pressure, and saturation state must also influence polytypism.

O'Hanley (1991) described variations in serpentine-mineral (lizardite, antigorite, chrysotile, and polygonal serpentine) distribution with proximity to fault zones and the importance of faults and fractures in controlling the access of fluids needed in olivine + enstatite → serpentine reactions. However, a direct connection between complex polytypism and deformation was not proposed. Some corroborating evidence for such a link might be inferred from microbeam X-ray diffraction (XRD) camera results of Wicks and Whittaker (1977), who reported the common 1*T* polytype in pseudomorphic and nonpseudomorphic serpentines but multilayer polytypes in slickensided veins. Although it has been shown that mechanical grinding during sample preparation for XRD experiments can change the chlorite polytype (Shirozu, 1963), relationships between deformation and polytypism have not been explored.

Planar polytypes of 1:1 layer silicates were proposed by Newnham (1961), Zvyagin (1962, 1967), Steadman (1964), Zvyagin et al. (1966), Bailey (1969), Dornberger-Schiff and Ďurovič (1975a, 1975b), and Ďurovič et al. (1981). Polytypism in 1:1 layer silicates arises because stacking of these layers varies in two fundamental ways. First, cations occupy one of two sets of positions (I or II), which results in one of two octahedral slants. Set I is related to II by a 180° rotation. Structural variations arise when layer sequences involve combinations of type I and II octahedra. The second source of polytypic variation is the positioning of adjacent planar layers in one of three ways to ensure H bonding. The sixfold rings can exactly superimpose along **c** (zero shift) or be shifted by **a**/3 along the three pseudohexagonal **a** axes (the sense of shift is determined by whether cations in the underlying layers are type I or II) or ±**b**/3 along the three **b** axes.

Various assumptions were made in all polytype derivations to limit the number of possible structures. Bailey's (1969) derivation of the 12 standard 1:1 layer silicate polytypes was achieved by excluding structures with shifts along both **a** and **b** and those with both zero and ±**b**/3 or ±**a**/3 mixed in the same crystal. In the vast majority of studies, serpentine polytypes identified by standard powder XRD techniques are reported to be one of the 12 standard polytypes (Bailey, 1969), 1*T* being the most common. However, structures containing more complex sequences do form under some conditions (e.g., the $6R_2$ polytype reported by Steadman and Nuttall, 1962, and the $6T_1$ polytype inferred for Unst serpentine by Hall et al., 1976). Results presented here illustrate that, under some circumstances, these polytypes may be important constituents of assemblages of 1:1 layer silicates.

Polytypes based on ±**b**/3 displacements and characterized by long-period regular stacking must involve more complex sequences of displacements, including sequences that intermix zero and ±**b**/3 displacements (simply referred to below as 0, +, or −). Possible sequences for all three- and four-layer structures (excluding regular **a**/3 displacements) are listed by Bailey and Banfield (1995), who describe the procedure to identify three- or four-layer polytypes (regular stacking involving zero or **b**/3 shifts, regardless of slant of octahedra, $\beta = 90°$). Their method involves recognition of the high-intensity (or missing) 02*l* reflections, regardless of whether the [100], [110], or [1$\bar{1}$0] zone is obtained. Bailey and Banfield (1995) also calculated diffraction data for 1:1 layer silicates with long-period order in the octahedral cation sequence (up to seven layers) and provided criteria on the basis of 20*l* intensity data to identify each sequence uniquely. Here we use results from this theoretical study to decipher the detailed structures of previously undescribed polytypes.

Lizardite, antigorite, and chrysotile are varieties of serpentine distinguished by the mechanisms they employ to relieve strain associated with lateral misfit between the tetrahedral and larger octahedral sheets (e.g., Pauling, 1930). Although polygonal serpentine (described as Povlen-type by Krstanović and Pavlović, 1964) is sometimes considered a fourth 1:1 layer structure (Mellini, 1986), most results suggest it is simply a special lizardite arrangement (high surface area may modify its stability relative to lizardite). Polygonal serpentine has been described from numerous localities. It is generally believed to have formed by modification of (and in some cases, overgrowth on) preexisting chrysotile (e.g., Cressey and Zussman, 1976; Mellini, 1986; Mitchell and Putnis, 1988).

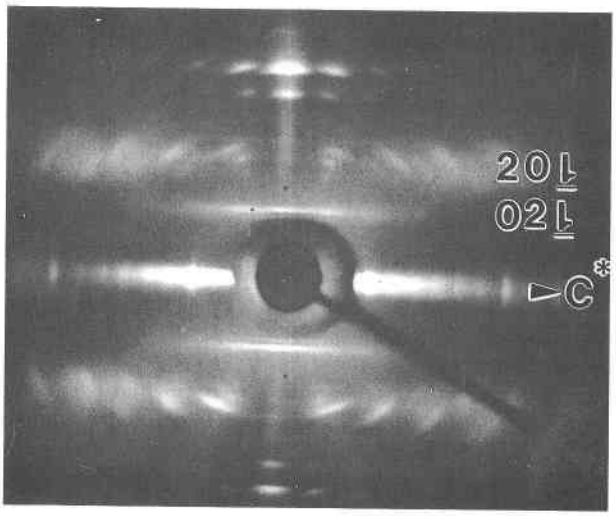

Fig. 1. XRD precession photograph supporting optical microscope and electron microscopic information indicating that layer silicates adopt one of two orientations. All crystals have **c*** normal to the foliation direction. Approximately one-half of the crystals have **b*** rather than **a*** parallel to the foliation direction.

There have been several attempts to explain why virtually all polygonal serpentines contain either 15 or 30 segments (Cressey and Zussman, 1976; Cressey, 1979; Yada and Liu, 1987; Mitchell and Putnis, 1988; Wicks and O'Hanley, 1988). Chisholm (1992) proposed a model based on geometric and strain considerations (particularly the addition of integral numbers of octahedra and tetrahedra to successive layers at sector boundaries). More recently, Baronnet et al. (1994) presented an elegant model for the growth of 15- and 30-sector polygonal serpentine. Baronnet et al. (1994) noted that the chrysotile-to-lizardite transition requires unit cells in successive layers to move into registry along the **b** axis to establish H bonding. Baronnet et al. (1994) proposed that the five additional unit cells per layer (needed to complete successively larger diameter layers) reorganize to form five edge dislocations that dissociate symmetrically, resulting in 15 arrays of partial edge dislocations that form the sector boundaries. The model predicts that 15-sector polygonal serpentine should be characterized by five sets of three-sector groups with specific polytypic characteristics.

In this paper we describe the planar and polygonal serpentine mineralogy of altered and highly deformed metamorphosed peridotite and propose a link between unusual polytypism and deformation. The importance of the structural characteristics of these serpentines, which represent precursors for associated regular serpentine-chlorite interstratifications, is explored in a companion paper (Banfield and Bailey, 1996).

Experimental methods

Samples

Samples are from the State Line serpentinite, which formed by metamorphism of an alpine-type peridotite that intruded into schists and gneisses in the Ordovician. The serpentinite is now exposed in the Woods Chrome Mine, Lower Britain Township, Lancaster County, Pennsylvania (Lapham, 1958). Specimens were collected circa 1955 (by R.C.S.) from mine dumps (39043′52″N, 76006′20″W) and correspond to the material termed chromian antigorite by Glass et al. (1959).

The Woods Chrome Mine produced at least 88000 metric tons of chromite from boudin-like pods in the latter part of the nineteenth century. Most of the chromite deposits were located within 100 m of the presently preserved base of the serpentinites of the Baltimore Mafic Complex (Hanan and Sinha, 1989). Zircons associated with monazite-(La) and baddeleyite in clinochlore veins in this complex yielded slightly discordant age estimates of 510 Ma (A. A. Drake, personal communication to R.C.S.). Shaw and Wasserburg (1984) reported an age of 490 ± 20 Ma for igneous crystallization. Serpentinized dunites and gabbros were described by McKague (1964). In addition, the complex includes a continental margin island arc or back arc (the James Run formation; Hanan and Sinha, 1989), the Port Deposit Tonalite, and associated melange (including the Bald Friar metabasalt and the Conowingo Creek metabasalt). Together, these units represent an ophiolitic island arc complex that was obducted onto Laurentia during the closure of the Iapetus during the Taconic orogeny at approximately 455 Ma. It is probable that the chromian serpentinites formed during the deformation and metamorphism that accompanied the Taconic obduction and thrusting.

Most of the chromite ore in the Woods Chrome Mine contained 48 wt% Cr_2O_3. An analysis of the serpentinized dunite from a nearby quarry yielded SiO_2 37.3%, Al_2O_3 0.15%, total Fe as FeO 6.3%, MgO 39.3%, CaO 0.23%, MnO 0.08%, K_2O 0.06%, Na_2O 0.01%, NiO 0.3% (McKague, 1964). The ore boudins were reported typically to be surrounded by a 1 m thick sheath of translucent green Ni-bearing antigorite. Chromian chlorite and chromian serpentine, the latter typically having a cross-fiber or slickensided habit, occurred in vein or breccia fillings in brittle fractures in the chromite. Other minerals include common brucite, clinochlore, and dolomite; trace maucherite, millerite, pentlandite, and zaratite; and rare uvarovite. The serpentinite consists of 81% serpentine-group minerals, 5% olivine (Fo_{95}), 6% opaque minerals, 1% chromite, 1% talc, 2% carbonate minerals, 1% brucite, the remainder being chlorite and other minerals. Textural relations reported by Lapham (1958) suggest serpentinization preceded chloritization.

Characterization of the layer silicate assemblage

Powder and precession XRD patterns were obtained from serpentine minerals. Three-millimeter diameter samples were removed from a thin section, mounted on copper support washers, and thinned to electron transparency by Ar ion milling. Samples were C coated before examination in a 200 kV Philips CM20 UT high-resolution transmission electron microscope (HRTEM) with

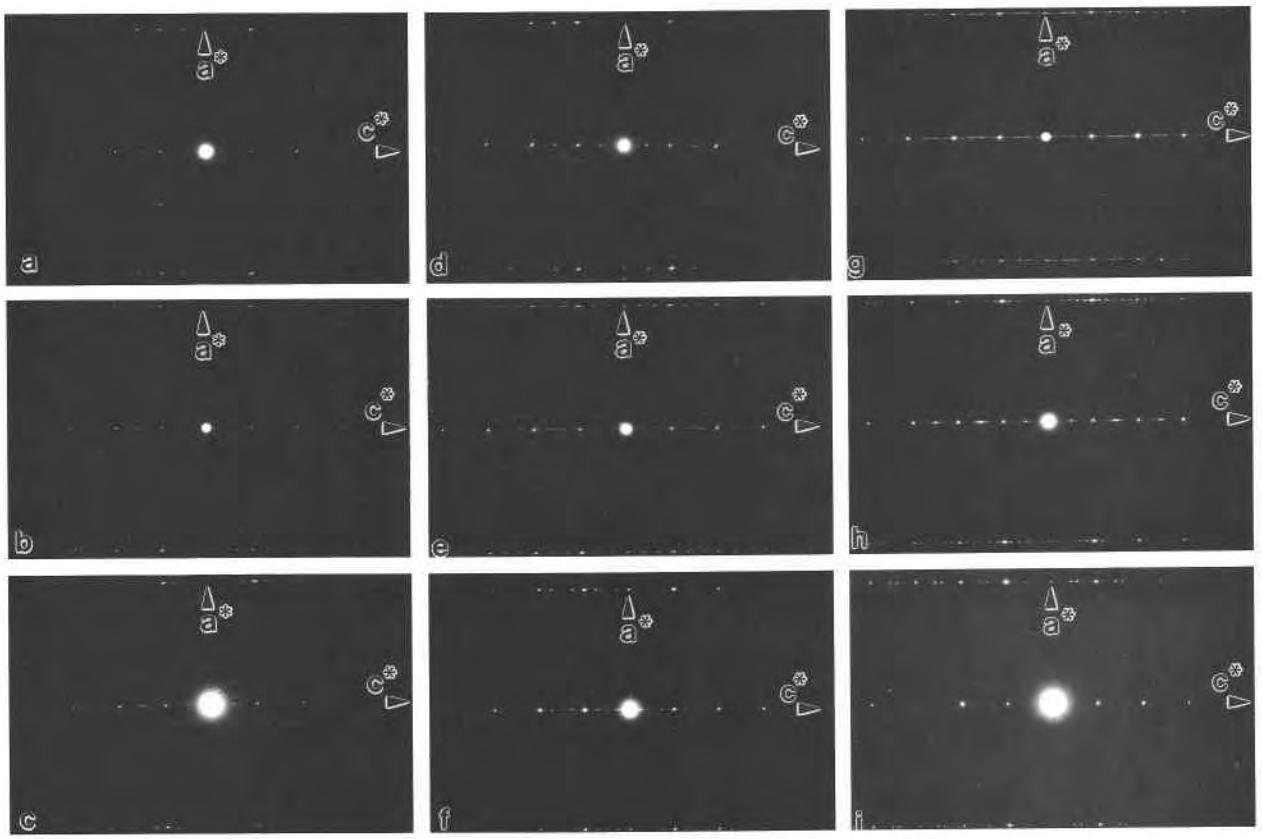

Fig. 2. The [010] SAED patterns of Cr-rich serpentine exhibiting order in the octahedral cation sequence: (**a**) two layer (I,II); (**b**) three layer (e.g., I,I,II); (**c**) four layer (I,I,II,II); (**d–f**) duplicate **a–c** from a thicker area (note the stronger dynamical effects in **d–f**); (**g**) five layer; (**h**) six layer; (**i**) seven layer (nine layer pattern not shown). Continuous streaking of $0kl$, $k \neq 3n$ reflections in all [100] SAED patterns indicates disorder in **b**/3 (and possibly **a**/3) displacements between successive 1:1 layers.

a point resolution of about 0.19 nm. Ten ion-milled samples were examined. Compositional analysis in the HRTEM was performed using a NORAN Ge detector and NORAN Voyager software. Tilt capabilities of the CM20 UT ($\alpha = \pm 15°$, $\beta = \pm 20°$) were just sufficient to allow both [010]-type and [100]-type selected-area electron diffraction (SAED) patterns to be obtained from the same crystal under the most favorable conditions (e.g., [010] as well as [$\bar{1}$10]).

Images were interpreted by comparison with image simulations calculated using EMS (Stadelmann, 1991). The $00l$ periodicities in SAED patterns oriented to eliminate dynamical diffraction effects involving $20l$ rows were used to distinguish layer silicates. In cases of standard serpentine and chlorite polytypes, identification was established by comparison with calculated and observed patterns reported by Bailey (1988b). Octahedral sequences were analyzed from [010] SAED patterns by interpreting variations in intensity of $20l$ reflections, which are sensitive to octahedral cation order and essentially unaffected by variations in stacking order (Bailey and Banfield, 1995). Identification of stacking sequences in nonstandard three- and four-layer polytypes involved matching experimental SAED patterns with those calculated for samples between 3 and 20 nm in thickness by Bailey and Banfield (1995). This analysis assumes polytypes do not contain regular shifts of $\pm$**a**/3. SAED patterns were recorded from the thinnest possible areas (probably usually 7–10 nm thick). Calculations reveal that, in most cases, distinct intensity variations were not greatly obscured by dynamical diffraction effects in samples up to 10 nm thick.

Results and interpretation

General sample description

Specimens are mauve in color because of the significant Cr content of all minerals. Strongly foliated samples display a distinct lineation in the foliation plane. Specimens break into elongate, blocky aggregates with the lineation parallel to the length of the fragments. Petrographic optical examination of fragments down Z reveals that optically continuous millimeter-sized regions have extinction directions approximately parallel and perpendicular to the lineation direction (generally $\pm 10°$). Furthermore, XRD photographs from subsamples show that, in addition to a common **c*** direction, the majority of crystals have either **a*** or **b*** parallel to the lineation (Fig. 1).

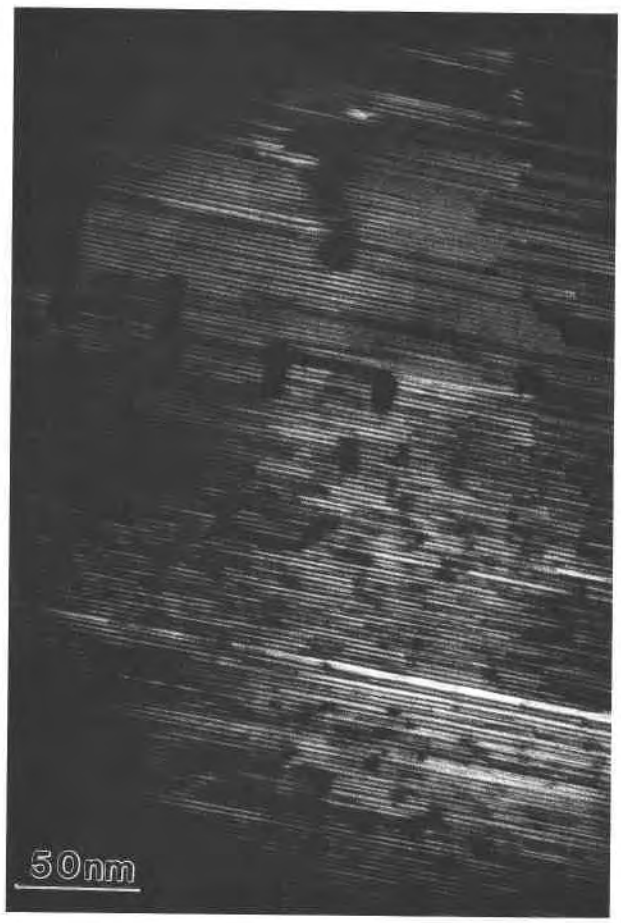

Fig. 3. Dark-field image from an area of serpentine showing a three-layer 20*l* periodicity. The regular periodicity is interpreted to indicate a high degree octahedral cation order.

Reflections are arc shaped, suggesting some (~15°) misorientation. The strong preferred orientation is also apparent when samples are examined in the electron microscope.

Thin section examination revealed that samples are comprised almost entirely of layer silicate minerals peppered by small opaque crystals. The opaques, shown by analytical electron microscopy (AEM) to be chromite, occur in trails that parallel the lineation direction.

Powder XRD patterns could be indexed as derived from either a six-layer serpentine or from a mixture of dozyite (1:1 serpentine-chlorite; Bailey et al., 1995; Banfield et al., 1994), serpentine, and chlorite. XRD precession photographs suggest that the layer silicate assemblage is dominated by serpentine with a two-layer periodicity in 20*l* (regular alternation in adjacent layers of set I and set II octahedral cations). These could be either group B or group D serpentines, as classified by Bailey (1969). Group B serpentines are very rare, however, and none were identified in this study. Here we describe serpentines with semirandom stacking and a two-layer repeat in 20*l* reflections as two layer (I,II) and assume the stacking is based on displacements along the **b** (as in group D) rather than the **a** axis (as in group B).

Transmission electron microscopy

HRTEM images and SAED patterns indicate the sample consists of a complex assemblage of serpentine-group minerals as well as chlorite and large unit-cell structures that are based on regular interstratifications of serpentine and chlorite. Within the resolution of the energy-dispersive X-ray analytical technique, all minerals have the same Mg-rich, Al- and Cr-bearing, Fe-poor compositions. The chlorite (I*bb*) and regular serpentine-chlorite interstratifications, their microstructures, reaction mechanisms, and origins are discussed in a companion paper (Banfield and Bailey, 1996).

The serpentine-group minerals in this sample can be subdivided into three categories. The most abundant are polytypes of planar serpentine. Of lesser abundance are antigorite and polygonal serpentine.

Planar serpentine

The most common serpentine in the assemblage has continuously streaked 0*kl*, $k \neq 3n$ reflections and a two-layer repeat in 20*l* (Fig. 2a and 2d). In [100] images, displacements of **a**/3 along the **a** and pseudo-**a** axes (such as found in group B) and **b**/3 along the pseudo-**b** axes (as found in group D) both have projected displacements of zero or **b**/6. Thus, HRTEM image details cannot be used to distinguish disordered **a**/3 from **b**/3 stacking. As noted above, we assume the displacements are along **b**.

There are two distinct categories of planar serpentines, each of which contains members that exhibit long-period polytypes not described previously. Both groups have $\beta = 90°$. The first group (1) has a periodicity of ≥0.7 nm in 20*l* reflections (Fig. 2), indicating octahedral order (Fig. 3) and 0*kl*, $k \neq 3n$ reflections that are continuously streaked (see Fig. 4a). The second group (2) is characterized by periodicities of ≥1.4 nm in 20*l* and discrete spots rather than streaks in the 0*kl*, $k \neq 3n$ rows, indicating regular sequences of **b**/3 displacements between adjacent 1:1 layers (Fig. 4). Serpentines with regular stacking have either $\alpha \neq 90°$ (triclinic symmetry) or $\alpha = 90°$ (monoclinic or triclinic symmetry). In all patterns from serpentine (00*l* periodicity = 0.7 nm) with a 20*l* period > 2.8 nm, the 0*kl*, $k \neq 3n$ reflections are continuously streaked.

Polytypes with disordered stacking. Some serpentines display a 0.7 nm periodicity in 20*l* (group C: I,I,I . . . octahedral tilts). The [010] SAED patterns normally exhibit multiples of the 0.7 nm periodicity in 20*l* rows. A two-layer periodicity is most common (Fig. 2a) and can be distinguished from patterns from regularly interstratified minerals (2.1–6.3 nm periodicities in 00*l* and 20*l*; see Banfield and Bailey, 1996) only if the patterns are from the very thinnest areas or if crystals are subsequently tilted so that 20*l* reflections are not diffracting strongly.

Patterns with a three-layer (2.1 nm) periodicity in 20*l* are relatively common (Fig. 2b and 2e). Calculated SAED

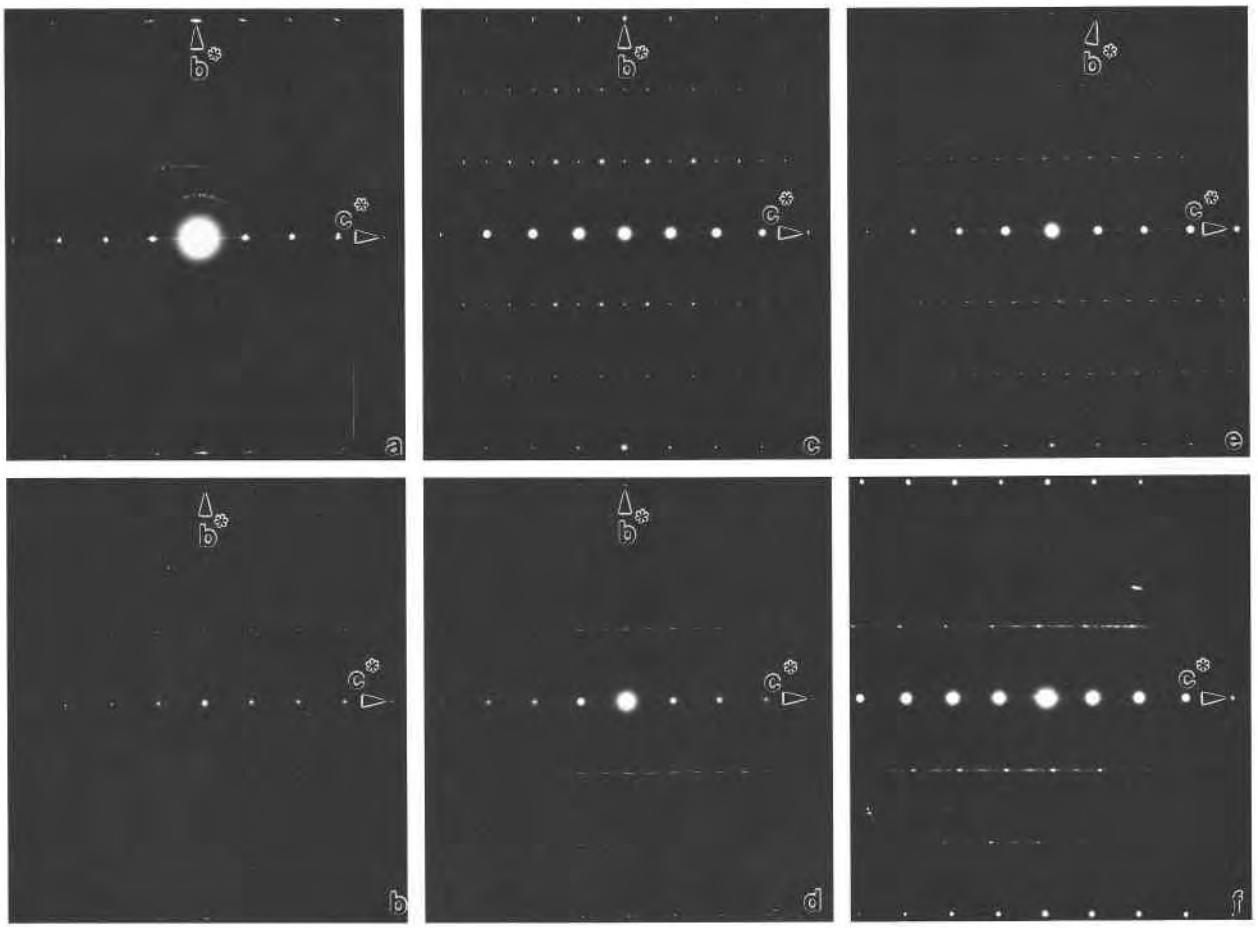

Fig. 4. The [100] SAED patterns of standard polytypes of Cr-rich serpentine: (**a**) disordered stacking; (**b**) $2H_1$; (**c**) $2T$; (**d**) $2H_2$; (**e**) $6R_2$; (**f**) $6R_1$. All polytypes except $2T$ (group C) show a two-layer period in $20l$ (group D).

patterns show that $20l$ periodicities and intensities are independent of the sequence of **b**/3 displacements between adjacent 1:1 layers. Calculations demonstrate that a 2.1 nm periodicity can be explained only by a sequence in which the octahedral slants alternate in a I,I,II-type sequence (Bailey and Banfield, 1995). Although calculated $20l$ and $20\bar{l}$ intensities are quite different (Bailey and Banfield, 1995), SAED patterns (Fig. 2b) have approximate mirror symmetry. The match between the experimental and calculated pattern is much improved if 180° twinning (superimposing $20l$ and $20\bar{l}$) is invoked.

SAED patterns for serpentines with a four-layer repeat in $20l$ exhibit two distinct patterns of $20l$ intensities. Comparison with calculated patterns reported in Bailey and Banfield (1995) indicates that those with intense satellites on the 0.7 nm subcell reflection (Fig. 2c and 2f)

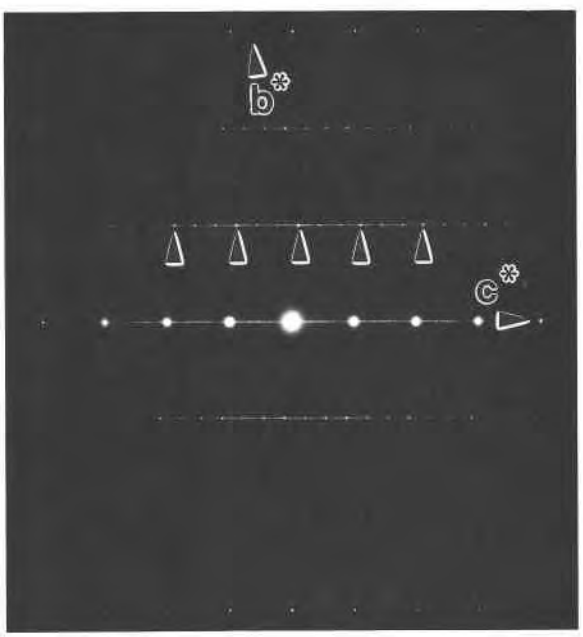

Fig. 5. The [100] SAED pattern from serpentine characterized by three-layer periodicity in $0kl$, $k \neq 3n$, and $\alpha = 98°$. Arrows indicate the strongest $02l$ reflections.

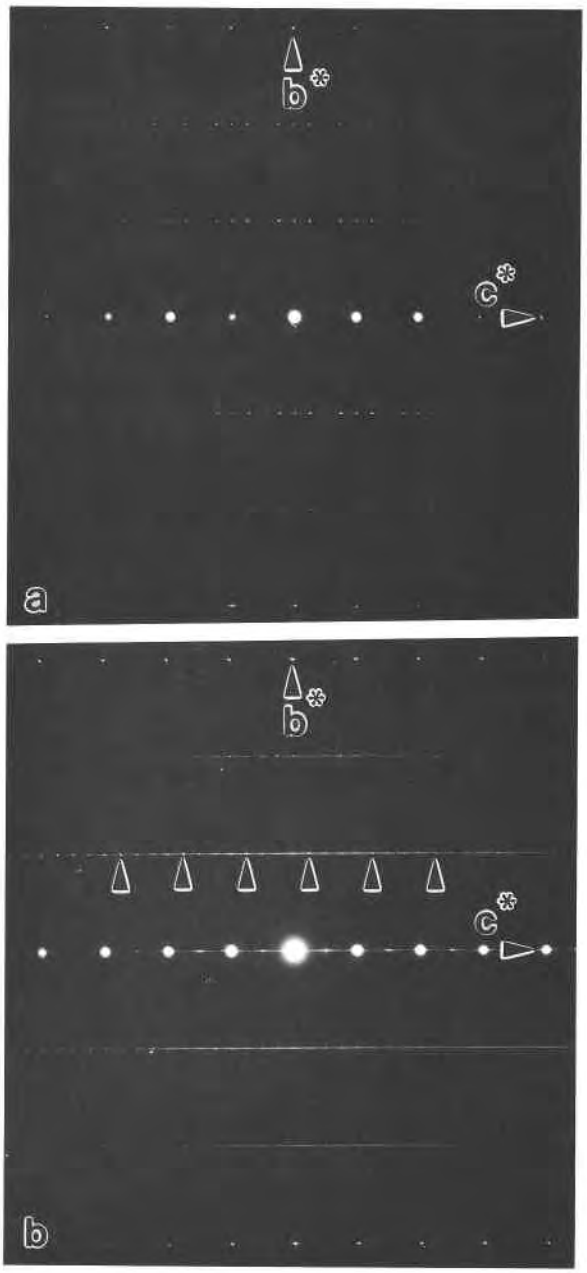

Fig. 6. The [100] SAED patterns from serpentine characterized by four-layer periodicities in $0kl$, $k \neq 3n$, and $\alpha = 90°$; (**a**) 0,−,0,+ and (**b**) −,−,−,0. Arrows in **b** indicate the strongest $02l$ reflections.

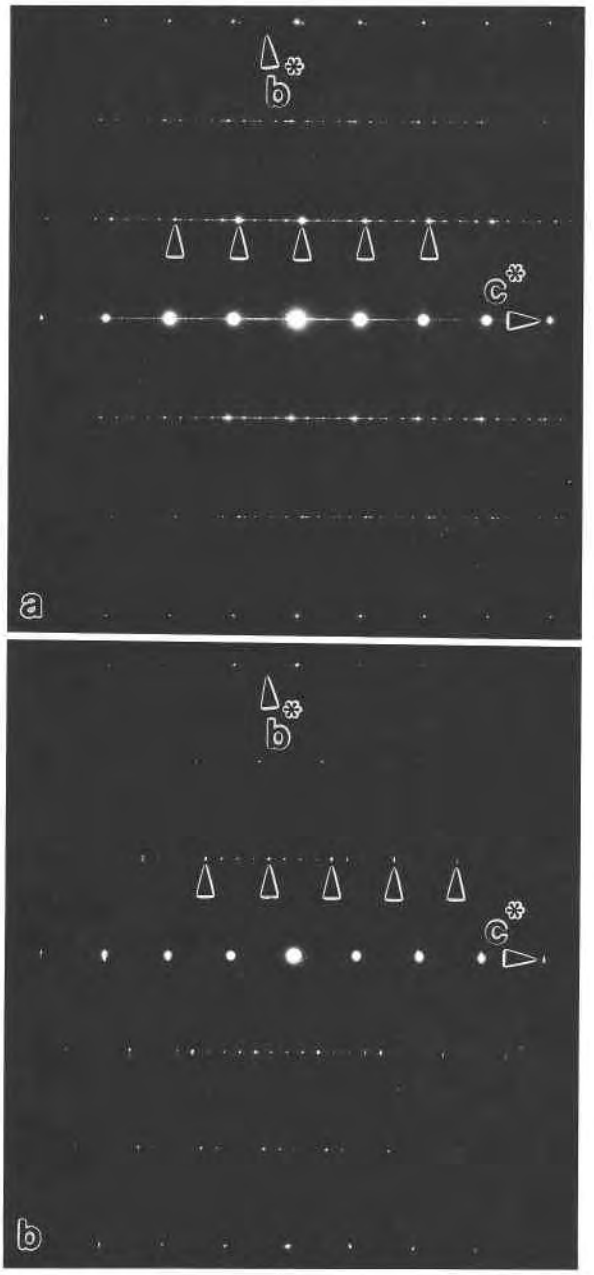

Fig. 7. The [100] SAED patterns from serpentine characterized by four-layer periodicities in $0kl$, $k \neq 3n$, and $\alpha = 96°$; (**a**) 0,0,0,− and (**b**) +,+,+,−. Arrows indicate the strongest $02l$ reflections.

are derived from serpentine in which the octahedral cations alternate in a I,I,II,II pattern, whereas those with uniform $201 \approx 202 \approx 203$ intensities are from serpentines with regular I,I,I,II alternation of octahedral cations.

Serpentines with five-layer (Fig. 2g), six-layer (Fig. 2h), seven-layer (Fig. 2i), and nine-layer (not shown) repeats in the $20l$ reflections must have 3.5, 4.2, 4.9, and 6.3 nm periodicities in their octahedral cation sequences. Patterns show distinct intensity variations that can be matched with the results of Bailey and Banfield (1995) to identify uniquely the following sequences: I,II,I,II,II; I,I,I,II,II,II; I,II,I,II,I,II,II; and I,II,I,II,II,II,II (the nine-layer structures were not analyzed).

Images formed using $20l$ reflections in close to two-beam conditions (e.g., using two strongly diffracting $20l$ reflections) indicate a very high degree of octahedral order (especially for three- and four-layer serpentines) over large areas (Fig. 3). In some regions, the 2.1 nm period-

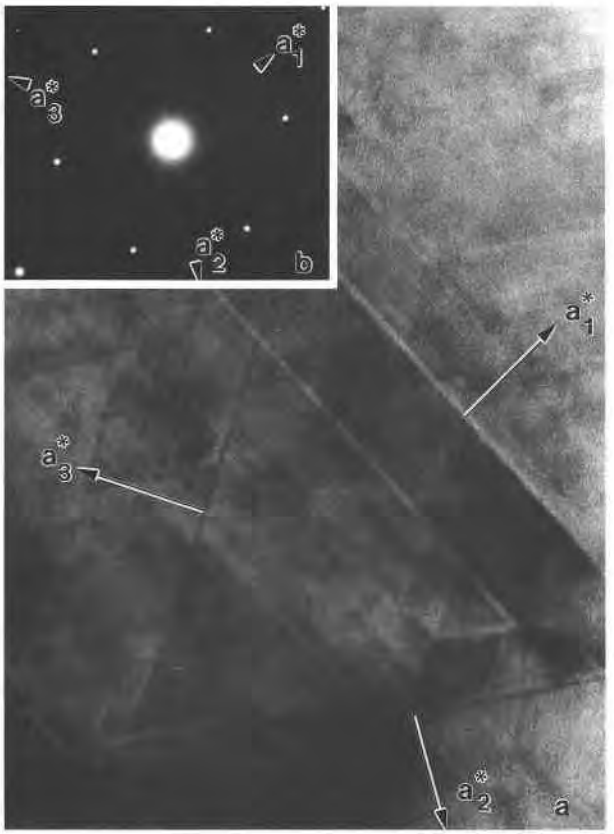

Fig. 8. (**a**) Image down [001] illustrating defects perpendicular to the real **a*** and pseudo-**a*** axes. (**b**) SAED pattern for **a**. Careful examination of diffraction spots indicates they are star shaped with streaks perpendicular to defect orientations.

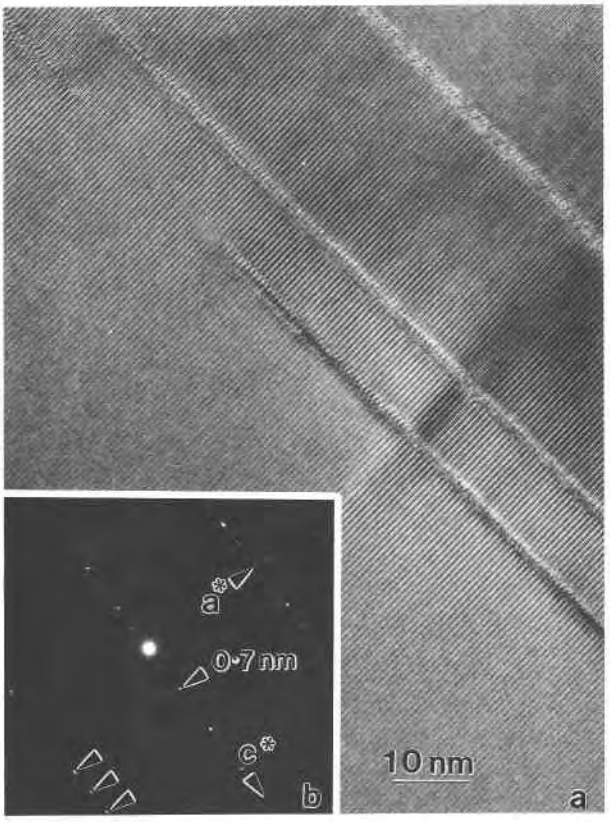

Fig. 9. (**a**) Image down [010] illustrating serpentine crosscut by planar defects perpendicular to **a***. Sighting at a low angle along the fringes indicates a displacement in 1.4 nm fringes under some thickness and tilt conditions. (**b**) SAED pattern illustrating that the serpentine has a two-layer period (see arrows) in 20*l*. The weak 1.4 nm reflection in the 00*l* row is due to dynamical diffraction.

icity is modulated every three unit cells, producing a 6.3 nm periodicity. In rare areas, images indicating imperfect periodicities of up to 50 nm were recorded.

Polytypes with regular stacking. Stacking order is indicated by discrete 0*kl*, $k \neq 3n$ reflections. For crystals with a 1.4 nm 02*l* periodicity, polytypes established by comparison with results of Bailey (1988b) and Bailey and Banfield (1995; for the case of $6R_2$) were $2H_1$ (group D, Fig. 4b), $2T$ (group C, Fig. 4c), $2H_2$ (group D, Fig. 4d), $6R_2$ (group D, Fig. 4e), and $6R_1$ (group D, Fig. 4f). In some cases, these crosscut well-ordered (e.g., $2H_1$ crosscutting $6R_2$) and randomly interstratified serpentine-chlorite crystals.

A triclinic unit cell with $\alpha = 98°$ was chosen for serpentines that exhibit a three-layer periodicity along 0*kl*, $k \neq 3n$ rows (i.e., a 2.1 nm periodicity in 02*l*). The position of the strongest 02*l* reflection is the same in each of the three-layer patterns recorded, indicating a single three-layer triclinic polytype (Fig. 5). On the basis of results reported by Bailey and Banfield (1995), the stacking sequence is determined uniquely to be 0,0,−. The 2.1 nm periodicity in 20*l* indicates a I,I,II octahedral cation sequence. It is probable that the $-\mathbf{b}/3$ displacement corresponds with the change from type I to type II octahedra.

Four types of SAED patterns, distinguished by the position of the strongest 02*l* reflection or an absent reflection, were obtained from the four-layer serpentine, indicating four distinct four-layer, regularly stacked sequences. A unit cell with $\alpha = 90°$ is appropriate for two groups of crystals with a 2.8 nm repeat in 02*l*, and a triclinic cell with $\alpha = 96°$ was selected for crystals with two other types of SAED patterns. Comparison between intensities calculated for model structures ($\alpha = 90°$) by Bailey and Banfield (1995) and those in Figure 6a clearly indicates regular 0,−,0,+ stacking, whereas intensities in Figure 6b indicate a regular −,−,−,0 sequence. Likewise, intensities in Figure 7a indicate regular 0,0,0,− stacking, and those in Figure 7b indicate +,+,+,− stacking. Although polytypes with four-layer regular stacking commonly have I,II octahedral cation sequences, patterns with I,I,II,II were also recognized.

Planar microstructures in serpentine. Planar serpentine frequently contains nonperiodic defects parallel to (100), (110), and (1$\bar{1}$0). Although these faults are commonly developed in approximately equal numbers parallel to each

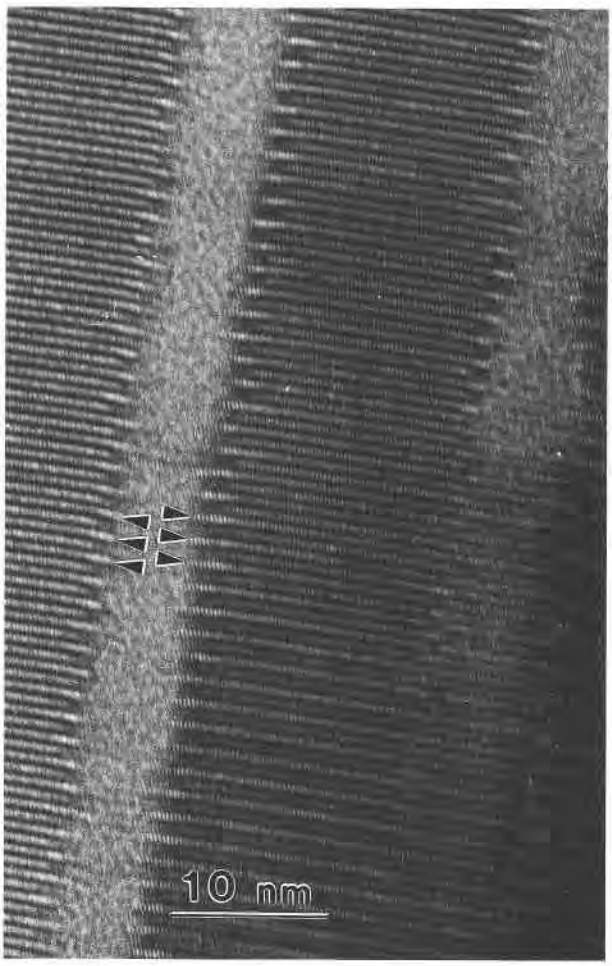

Fig. 10. High-resolution [010] image of serpentine surrounding beam-damaged regions associated with defects illustrated in Fig. 14. Arrows indicate that the two-layer periodicity is offset.

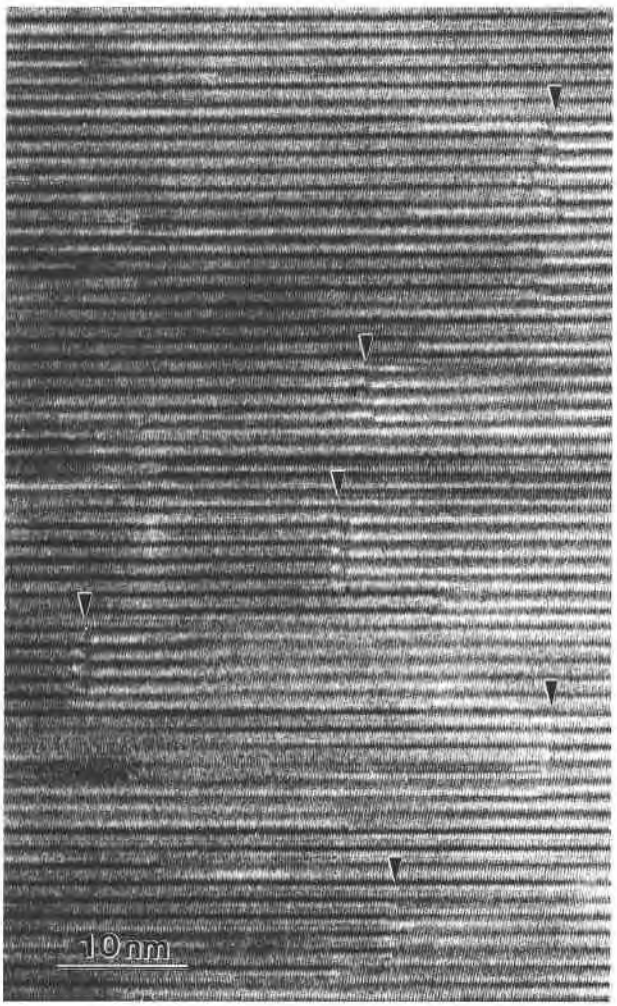

Fig. 11. High-resolution [010] image of discontinuous defects in two-layer serpentine. Details in contrast and fringe orientation suggest defects separate polytypically distinct sequences.

of these planes (Fig. 8), they occur in only one orientation in some areas. Faults may terminate without major structural disruption of surrounding serpentine, may be correlated in position across one packet of serpentine, and have a maximum width of ~3 nm (Fig. 9). In some areas, fringes are apparently offset across faults and in others they are not (Fig. 9). Rotation of fringes by a few degrees across the faulted region occurs in some areas. Faults are especially prone to beam damage, so that it is difficult to record images that reveal their detailed structure (Fig. 10). Comparison between ordering patterns on either side of the zone suggests that, at least in some cases, faults separate regions in which the polytypic sequence is out of phase (Fig. 10) or is quite different (Fig. 11). Distinct patterns of serpentine-chlorite are sometimes observed on either side of the fault, suggesting that chlorite nucleation postdated development of the planar faults.

Antigorite

The sample contains small (usually <0.2 μm in length and width) antigorite crystals that are both concordant (Fig. 12) and discordant with respect to surrounding planar serpentine. Small crystals that crosscut the planar serpentine and serpentine-chlorite probably postdate the chloritization event. Images and [010] SAED patterns from antigorite crystals indicate a ~5 nm modulation periodicity approximately parallel to **a***. Groups of satellites around the main serpentine reflections form lines that deviate from **a*** by $<1°$. On the basis of the work of Spinnler et al. (1984) and Otten (1993), the negligible deviation of the direction of modulation periodicity from **a*** in SAED patterns is interpreted to indicate relatively defect-free crystals formed during late-stage alteration.

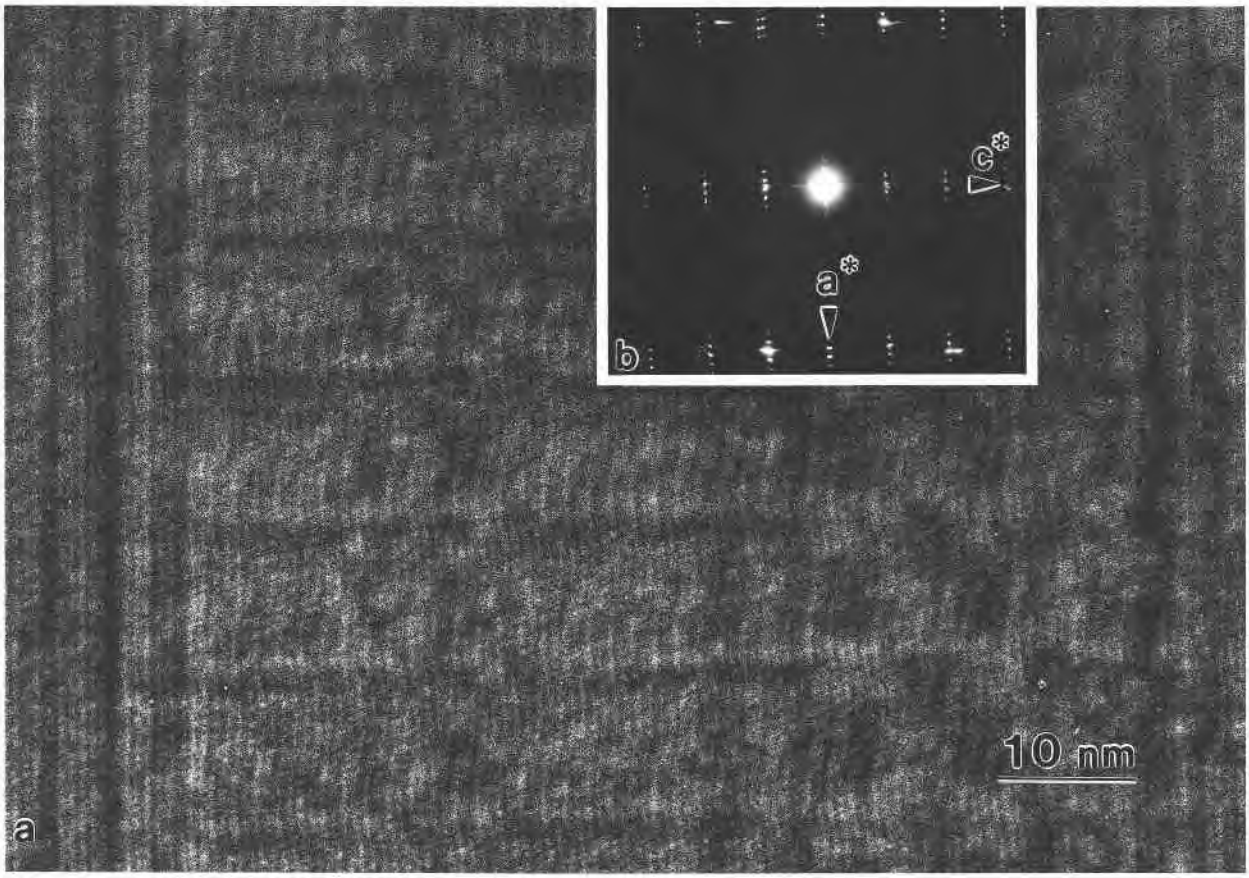

Fig. 12. (**a**) HRTEM image down [010] illustrating antigorite intergrown with lizardite. The SAED pattern in **b** indicates a ~5 nm antigorite modulation. Rows of satellites deviate <1° from **a***, indicating that antigorite is relatively perfect (e.g., Otten, 1993).

Polygonal serpentine

In some regions, planar serpentine polytypes and interstratified serpentine-chlorite are crosscut by regions partially filled by polygonal serpentine (Fig. 13). Sectors generally emanate from a single point that is commonly located on a surface step on planar serpentine. Within an individual sector, **b** is parallel to the layers and **a** parallels the tube axis, as in normal chrysotile. Occasionally, chrysotile coexists with polygonal serpentine (Fig. 14a). In some areas, sectors serve to link adjacent layer silicate packets in different orientations (Figs. 13 and 14). Variations in fringe periodicities in thicker areas indicate mixtures of polytypes.

In many cases, the two-layer serpentine (I,II) is characterized by random **b**/3 (and possibly **a**/3) displacements between adjacent layers. However, polygonal segments with regular stacking are also present. Where regular stacking is observed, polygonal arrangements consist of repeating patterns of three sectors (five sets of a three-sector sequence for complete polygonal units). Most commonly, pairs of enantiomorphic sectors ($6R_2$ or $2M_2$-pseudo-**a***-**c***) are separated by sectors with $\alpha = 90°$ (some areas, $2H_1$ or $2Or$; other areas, $2H_2$ or $2Or$-pseudo-**b***-**c***; Figs. 15 and 16). It is unlikely that group B and D polytypes are mixed in polygonal units. On the basis of the abundance of group D polytypes, we suggest the most common arrangement involves repetition of the sequence $6R_2$, $6R_2$-enantiomorph, $2H_2$ (Fig. 16). This pattern is consistent with predictions of Baronnet et al. (1994), unlike the alternative consisting of group B structures ($2M_2$-pseudo-**a***-**c*** enantiomorphs plus $2Or$-pseudo-**b***-**c***). In the former case, the $02l$ intensity patterns indicate that **b*** of adjacent $6R_2$ polytype sectors superimpose, so that a common **c**-axis direction parallels the sector boundary.

For cases where the sector between the enantiomorphic pairs has a one-layer period in $02l$, our results are consistent with the predictions of Baronnet et al. (1994) only if the sectors are all group B serpentines (enantiomorphic $2M_2$-pseudo-**a***-**c*** pairs plus $2Or$). The {062} surfaces (for the $2H_1$ or $2Or$ polytype, and related planes for other polytypes) form grain boundaries between adjacent sectors and separate sectors from planar serpentine-chlorite crystals.

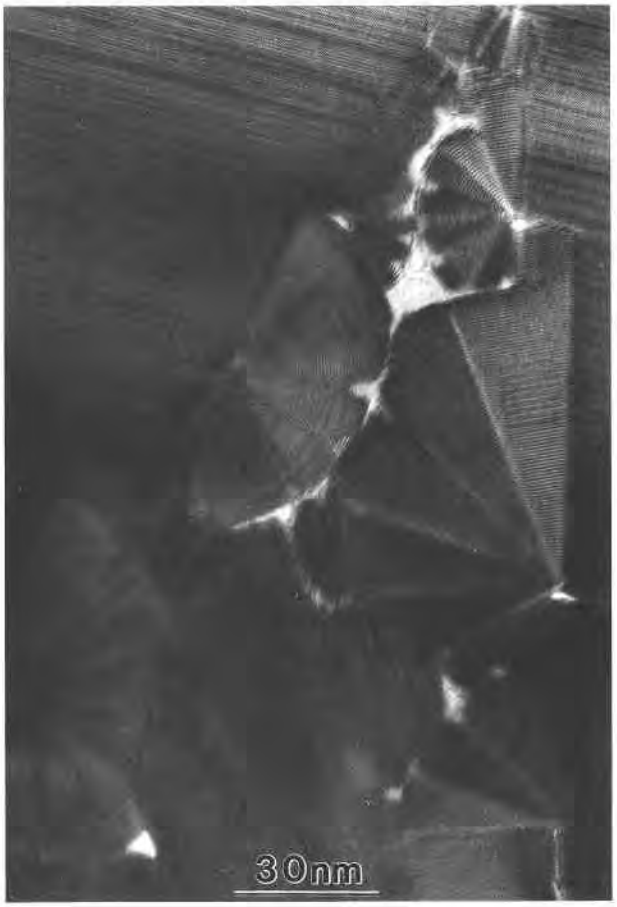

Fig. 13. Image down [100] illustrating polygonal serpentine in a zone that crosscuts planar serpentine. Polygonal crystals appear to have nucleated at steps on the surface of the planar serpentine.

Fig. 14 (above and right). The [100] images of polygonal serpentine. (**a**) Polygonal segments bridge planar serpentine. Beam damage is concentrated at segment interfaces. A indicates antigorite, and C indicates chrysotile-like serpentine. (**b**) Polygonal serpentine developed at grain boundaries between planar serpentine-chlorite intergrowths. Arrows in the top right corner indicate that (inclined) planar faults on (100) may be antiphase boundaries between chlorite units and separate serpentine and chlorite.

Discussion and conclusions

Serpentine polytypism

Comparison between calculated (Bailey and Banfield, 1995) and observed SAED patterns indicates that procedures for deciphering polytypic stacking and octahedral sequences in 1:1 layer silicates on the basis of recognition of strong or missing reflections are feasible if patterns are obtained from thin areas where the effects of dynamical diffraction are minimized. Using this approach, we determined that the serpentine mineralogy of sheared samples of the Cr-rich State Line serpentinite is distinctive in two important ways. First, the polytypic assemblage is diverse. Table 1 lists 21 different planar serpentine structures identified in our study. Second, the assemblage is characterized by less common structures, including at least 14 polytypes not recognized previously.

SAED patterns and dark-field images indicate that serpentine octahedral cations are highly ordered. However, the degree of stacking order is variable. Table 1 lists ten octahedral cation sequences. More complex sequences can be considered as based on the group D pattern of alternation of octahedral tilts with a mistake (twin?) every few unit cells or as intergrowths of groups C and D serpentine.

Although it is possible that group C serpentines are stabilized by lower Al contents, no compositional differences between polytypes were noted by analytical electron microscopy. However, subtle variations (e.g., in Al content) may have gone undetected. The long-period octahedral cation sequences and ordered stacking might have

Fig. 14. *Continued*

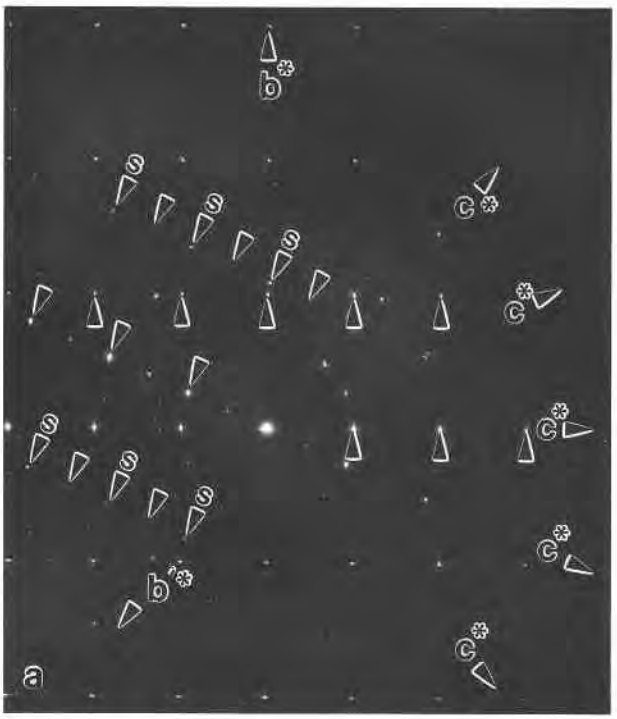

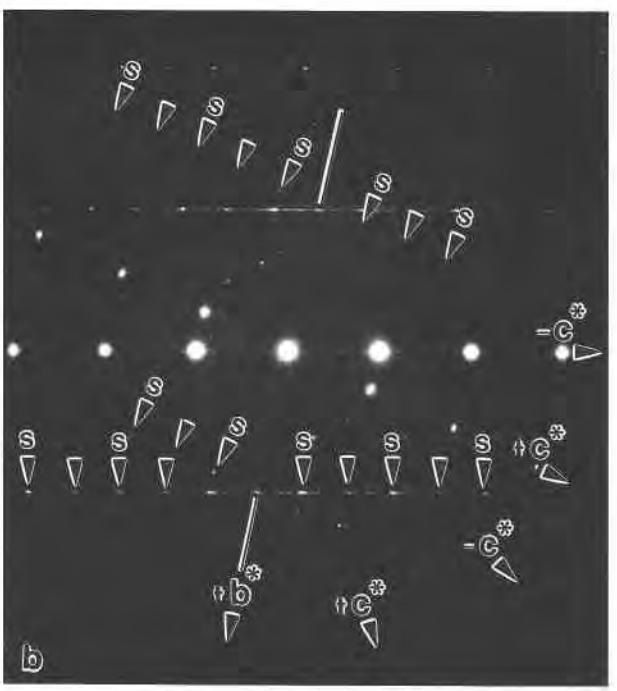

Fig. 15. SAED patterns of polygonal serpentine. (**a**) Adjacent segments consist of different polytypes. Note the one-layer period in $02l$ for the sector with $\alpha = 90°$ (see text). (**b**) Adjacent enantiomorphic segments (probably $6R_2$). Note the alternation of positive and negative **c** axes and that **b*** is common for two adjacent segments.

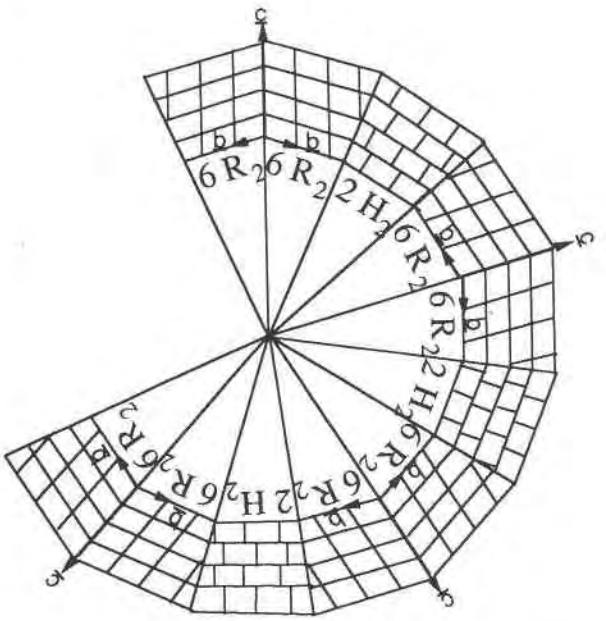

Fig. 16. Diagram illustrating the polytypic structure of polygonized serpentine as inferred from SAED patterns.

been established at the time of growth. Alternatively, the structures might have been modified subsequent to crystallization.

Polytypism and deformation

The most obvious macroscopic characteristic of the sample is that it displays a strong lineation within the foliation plane, indicating the sense of shear deformation. The lineation direction is approximately parallel to either **a** or **b** (and **a*** or **b***, as $\beta = 90°$) of the layer silicates. Overall, approximately equal numbers of crystals develop in the two orientations. This observation suggests that serpentine crystals were rotated during deformation or recrystallized in a shear environment. Thus, polytypic diversity might relate directly to the deformation.

In a series of papers, Baronnet and coworkers (e.g., Baronnet and Amouric, 1986; Baronnet, 1989; Baronnet and Kang, 1989) discussed the formation of long-period mica polytypes (ordered stacking) by growth controlled by screw dislocations in either a perfect or faulted matrix. Because relationships clearly exist between deformation, dislocations, and recrystallization, this mechanism might explain polytypic sequences if they were created during growth.

The alternative to primary polytypic diversity involves modification of original stacking sequences during deformation. This is plausible in our samples because the direction of shear corresponds to the direction in which layers must be displaced or O planes sheared to change one polytype into another. For example, for crystals that have **b** parallel to the shear direction, systematic interlayer displacements of **b**/3 (to optimize H bonding) could generate long-period polytypes characterized by regular

stacking (the regular I,II alternation of the majority of serpentines would be unaffected). Alternatively, the octahedral slant (i.e., I vs. II) could be reversed by shear of the OH planes in crystals with **a** parallel to the lineation (shear could also create **a**/3 stacking disorder, a possibility we were not able to rule out). Complex sequences of Is and IIs might be generated occasionally by periodic twinning or shear. This implies that macroscopic shear can, in some circumstances, be expressed microscopically as periodic displacements, e.g., displacement of $-\mathbf{b}/3$ every fourth layer (0,0,0,−). The detailed mechanism is not understood. It should be noted that an efficient mechanism for generation of long-period polytypes is not required because most crystals in the sample have disordered stacking, and long-period octahedral sequences are rare compared with two-layer structures.

At this time it is not known how common long-period serpentines are. Most previous polytypic characterization involved powder X-ray diffraction. Thus, it is possible that long-period serpentine structures are present as minor constituents of many assemblages but have been overlooked. This may be resolved by more routine polytypic characterization involving interpretation of SAED patterns using procedures described above. New data are required to test our hypothesis that more unusual and complex polytypes occur in deformed rocks.

Planar defects in serpentine

Faults are common microstructures in the planar serpentine (particularly group D serpentine), and they apparently predate chloritization. These defects share the orientation of antigorite-type reversals reported in lizardite by Livi and Veblen (1987). However, faults do not closely resemble antigorite offsets imaged at high resolution by Otten (1993) or shown in Figure 12. In some regions, faults terminate without any evidence in lattice fringe images for structural perturbation at the implied octahedral-octahedral and tetrahedral-tetrahedral (e.g., OT-TO or TO-OT) surfaces. Although we have not established that faults are regions where the polarity of the serpentine layers reverses, the much improved match between observed and calculated [010] SAED patterns if 180° twinning is invoked does support this interpretation.

Two-dimensional [010] lattice fringe images indicate that faults represent boundaries that separate serpentine regions in which the octahedral sequence is out of phase (e.g., I,II from II,I). Displacement of OH planes parallel to **a** within one region could create bounding faults normal to the three **a*** directions, resulting in triangular-shaped slabs of serpentine in which the octahedral slants are out of phase with surrounding areas (e.g., see Fig. 10). Such boundaries are also expected to be associated with screw dislocations where the Burgers vector has a magnitude equivalent to one layer and the octahedral periodicity is >1 layer. However, in a shear environment it seems improbable that abundant screw dislocations would develop normal to the shear direction (with the fault-cut planes in three orientations). Together, the polytypic structures and planar microstructures suggest that if octahedral sequences resulted from shear of OH planes, the process operated only within triangular-shaped subdomains.

TABLE 1. Serpentine polytypes

Disordered **b**/3 displacements	Ordered stacking	
One layer (group C)		
Two layer (I,II; group D)	$2T$	(−,+; I; group C)
Three layer (I,I,II)	$2H_1$	(0; I,II; group D)
Four layer (I,I,II,II)	$2H_2$	(−,+; I,II; group D)
Four layer (I,I,I,II)	$6R_1$	(−; I,II; group D)
Five layer (I,II,I,II,I)	$6R_2$	(0,−; I,II; group D)
Six layer (II,II,II,I,I,I)	$3Tc_1$	(0,0,−; I,I,II)
Seven layer (I,II,I,II,I,II,I)	$4M_1$	(0,−,0,+; I,II)
Seven layer (I,II,I,II,I,I,I)	$4Tc_1$	(0,0,0,−; I,II)
Nine layer not determined	$4Tc_2$	(−,−,−,+; I,II)
	$4Tc_3$	(0,−,−,−; I,II)
	$4Tc$?	(?; I,I,II,II)

Note: Group information refers to the group assigned to the standard polytypes by Bailey (1969). For polytypes with disordered **b**/3 displacements between adjacent layers, information in parentheses gives the sequence of octahedral cations, if known. For polytypes with ordered stacking, information in parentheses indicates the stacking sequence and sequence of octahedral cations. In all cases, $\beta = 90°$ (however, α may vary for three- and four-layer triclinic structures with regular stacking).

Polygonal serpentine

The development of polygonal serpentine in regions that crosscut serpentine-chlorite and at grain boundaries between adjacent planar serpentine crystals indicates that the polygonal sectors developed at a late stage in the peridotite alteration history. On the basis of angular relationships in SAED patterns, it can be deduced that if polygons were complete they would have 15 sectors, in accordance with previous observations of this mineral (e.g., Jiang and Liu, 1984; Mellini, 1986; Mitchell and Putnis, 1988; Yada and Liu, 1987; Baronnet et al., 1994). However, unlike most previous occurrences, polygons in our specimens have no open core. Direct restructuring of preexisting curved lizardite, such as that reported by Veblen and Buseck (1979), may have occurred. Polygonal units appear to have nucleated at steps on serpentine-chlorite surfaces, sometimes forming bridges between layers that terminate inclined crystals.

Baronnet et al. (1994) predicted sector polytypes based on the distribution of 15 partial dislocations (**b**/3) between the sectors, with resulting **b**/3 shifts between successive sectors around the fiber. The combination of $6R_2$ and $2H_2$ sectors is predicted by Baronnet et al. (1994), but the $6R_2$ and $2H_1$ combination is not. However, if the second case involves group B polytypes, the observed combination is consistent with the Baronnet et al. (1994) model. In general, our data support the view that the stacking sequence resulted from polygonization of chrysotile.

ACKNOWLEDGMENTS

Thanks are extended to Scott Sitzman for assistance with sample preparation and to Laurel Goodwin and Steven Ralser for helpful discussion.

This research was supported by NSF grants EAR-9117386 and EAR-9317082 to J.F.B. and a grant from the Department of Geology and Geophysics, University of Wisconsin–Madison to S.W.B. We thank Alain Baronnet and Huifang Xu for their careful reviews of this manuscript.

References cited

Amouric, M., and Baronnet, A. (1983) Effect of early nucleation conditions on synthetic muscovite polytypism as seen by high resolution transmission electron microscopy. Physics and Chemistry of Minerals, 9, 146–159.

Bailey, S.W. (1969) Polytypism of trioctahedral 1:1 layer silicates. Clays and Clay Minerals, 17, 355–371.

——— (1988a) Polytypism of 1:1 layer silicates. In Mineralogical Society of America Reviews in Mineralogy, 19, 725.

——— (1988b) X-ray diffraction identification of the polytypes of mica, serpentine, and chlorite. Clays and Clay Minerals, 36, 193–213.

Bailey, S.W., and Banfield, J.F. (1995) Derivation and identification of nonstandard serpentine polytypes. American Mineralogist, 80, 1104–1115.

Bailey, S.W., Banfield, J.F., Barker, W.W., and Katchan, G. (1995) Dozyite, a 1:1 regular interstratification of serpentine and chlorite. American Mineralogist, 80, 65–77.

Banfield, J.F., and Bailey, S.W. (1996) Formation of regularly interstratified serpentine-chlorite minerals by tetrahedral inversion in long-period serpentine polytypes. American Mineralogist, 81, in press.

Banfield, J.F., Bailey, S.W., and Barker, W.W. (1994) Polysomatism, polytypism, microstructures and reaction mechanisms in regularly and randomly interstratified serpentine and chlorite. Contributions to Mineralogy and Petrology, 117, 137–150.

Baronnet, A. (1975) Growth spirals and complex polytypism in micas: I. Polytype structure generation. Acta Crystallographica, A31, 345–355.

——— (1989) Polytypism and crystal growth of inorganic crystals. In H. Arend and J. Hulliger, Eds., Crystal growth in science and technology, p. 197–204. Plenum, New York.

Baronnet, A., and Amouric, M. (1986) Growth spirals and complex polytypism in micas: II. Occurrence frequencies in synthetic species. Bulletin Minéral, 109, 489–508.

Baronnet, A., and Kang, Z.C. (1989) About the origin of mica polytypes. Phase Transitions, 16/17, 477–493.

Baronnet, A., Mellini, M., and Devouard, B. (1994) Sectors in polygonal serpentine: A model based on dislocations. Physics and Chemistry of Minerals, 21, 330–343.

Bigi, S., and Brigatti, M.F. (1994) Crystal chemistry and microstructures of plutonic biotite. American Mineralogist, 79, 63–72.

Brown, B. E., and Bailey, S.W. (1962) Chlorite polytypism: I. Regular and semi-random one-layer structures. American Mineralogist, 47, 819–850.

Chisholm, J.E. (1992) The number of sectors in polygonal serpentine. Canadian Mineralogist, 30, 355–365.

Cressey, B.A. (1979) Electron microscope studies of serpentine textures. Canadian Mineralogist, 17, 741–756.

Cressey, B.A., and Zussman, J. (1976) Electron microscopic studies of serpentinites. Canadian Mineralogist, 14, 307–313.

Curtis, C.D., Hughes, C.R., Whiteman, J.A., and Whittle, C.K. (1985) Compositional variation within some sedimentary chlorites and some comments on their origin. Mineralogical Magazine, 49, 375–386.

de Caritat, P., Hutcheon, I., and Walshe, J.L. (1993) Chlorite geothermometry: A review. Clays and Clay Minerals, 41, 219–239.

Dornberger-Schiff, K., and Ďurović, S. (1975a) OD-interpretation of kaolinite-type structures: I. Symmetry of kaolinite packets and their stacking possibilities. Clays and Clay Minerals, 23, 219–229.

——— (1975b) OD-interpretation of kaolinite-type structures: II. The regular polytypes (MDO-polytypes) and their derivation. Clays and Clay Minerals, 23, 231–246.

Ďurović, S., Miklos, D., and Dornberger-Schiff, K. (1981) Polytypism of kaolinite-type minerals: An aid to visualize the stacking of layers. Crystal Research Techniques, 16, 557–565.

Glass, J.J., Vlisidis, A.C., and Pearre, N.C. (1959) Chromian antigorite from the Wood's Mine, Lancaster County, Pennsylvania. American Mineralogist, 44, 651–656.

Hall, S.H., Guggenheim, S., Moore, P., and Bailey, S.W. (1976) The structure of Unst-type 6-layer serpentines. Canadian Mineralogist, 14, 314–321.

Hanan, B.B., and Sinha, A.K. (1989) Petrology and tectonic affinity of the Baltimore Mafic Complex, Maryland. In S.K. Mittwede and E.F. Stoddard, Eds., Ultramafic rocks of the Appalachian Piedmont. Geological Society of America Special Paper, 231, 1–18.

Hayes, J.B. (1970) Polytypism of chlorite in sedimentary rocks. Clays and Clay Minerals, 18, 285–306.

Jiang, S., and Liu, W. (1984) Discovery and its significance of Povlen-type hydrochrysotile. Acta Geologica Sinica, 58, 136–142.

Karpova, G.V. (1969) Clay mineral post-sedimentary ranks in terrigenous rocks. Sedimentology, 13, 5–20.

Krstanović, I., and Pavlović, S. (1964) X-ray study of chrysotile. American Mineralogist, 49, 1769–1771.

Lapham, D.M. (1958) Preliminary report on the chromite occurrence at the Wood Mine, Pennsylvania. Pennsylvania Geological Survey Progress Report, 153, 11 p.

Livi, K.J.T., and Veblen, D.R. (1987) "Eastonite" from Easton, Pennsylvania: A mixture of phlogopite and a new form of serpentine. American Mineralogist, 72, 113–125.

McKague, H.L. (1964) The geology, mineralogy, petrology, and geochemistry of the State Line Serpentinite and associated chromite deposits, 166 p. Ph.D. thesis, Pennsylvania State University, University Park, Pennsylvania.

Mellini, M. (1986) Chrysotile and polygonal serpentine from the Balangero serpentinite. Mineralogical Magazine, 50, 301–305.

Mitchell, R.H., and Putnis, A. (1988) Polygonal serpentine in segregation-textured kimberlite. Canadian Mineralogist, 26, 991–997.

Newnham, R.E. (1961) A refinement of the dickite structure and some remarks on polytypism in minerals. Mineralogical Magazine, 32, 683–704.

O'Hanley, D.S. (1991) Fault-related phenomena associated with hydration and serpentine recrystallization during serpentinization. Canadian Mineralogist, 29, 21–35.

Otten, M.T. (1993) High-resolution transmission electron microscopy of polysomatism and stacking defects in antigorite. American Mineralogist, 78, 75–84.

Pauling, L. (1930) The structure of chlorites. Proceedings of the National Academy of Science, 16, 578–582.

Shaw, H.F., and Wasserburg, G.J. (1984) Isotopic constraints on the origin of Appalachian mafic complexes. American Journal of Science, 284, 319–349.

Shirozu, H. (1963) Structural changes of some chlorites by grinding. Mineralogical Journal (Japan), 4, 1–11.

Spinnler, G.E., Self, P.G., Iijima, S., and Buseck, P.R. (1984) Stacking disorder in chinochlore chlorite. American Mineralogist, 69, 252–263.

Stadelmann, P. (1991) Simulation of HREM images and 2D CBED patterns using EMS software package. Software manual 12M-EPFL, Lausanne, Switzerland.

Steadman, R. (1964) The structure of trioctahedral kaolin-type silicates. Acta Crystallographica, 17, 924–927.

Steadman, R., and Nuttall, P.M. (1962) The crystal structure of amesite. Acta Crystallographica, 15, 510–511.

Veblen, D.R., and Buseck, P.R. (1979) Serpentine minerals: Intergrowths and new combination structures. Science, 206, 1398–1400.

Velde, B. (1965) Experimental determination of muscovite polymorph stabilities. American Mineralogist, 50, 436–449.

——— (1993) Chlorite polytype geothermometry. Clays and Clay Minerals, 41, 260–267.

Walker, J.R., and Thompson, G.R. (1990) Structural variations in chlorite and illite in a diagenetic sequence from the Imperial Valley, California. Clays and Clay Minerals, 38, 315–321.

Wicks, F.J., and O'Hanley, D.S. (1988) Serpentine minerals: Structures and petrology. In Mineralogical Society of America Reviews in Mineralogy, 19, 91–159.

Wicks, F.J., and Whittaker, E.J.W. (1977) Serpentine textures and serpentinization. Canadian Mineralogist, 15, 459–488.

Yada, K., and Liu, W. (1987) Polygonal microstructure of Povlen chrysotile observed by high resolution electron microscopy. Proceeding of

the Sixth Meeting of the European Clay Group, Seville, Spain, 596–697.

Yoder, H.S., and Eugster, H.P. (1955) Synthetic and natural muscovites. Geochimica et Cosmochimica Acta, 8, 225–280.

Zvyagin, B.B. (1962) Polymorphism of double-layer minerals of the kaolinite type. Soviet Physics-Crystallography, 7, 38–51 [translated from Kristallografiya, 7(1), 51–65, 1962].

——— (1967) Electron diffraction analysis of clay mineral structures, 364 p. Plenum, New York.

Zvyagin, B.B., Mishchenko, K.S., and Shitov, V.A. (1966) Ordered and disordered polymorphic varieties of serpentine minerals and their diagnosis. Soviet Physics-Crystallography, 10, 539–546 [translated from Kristallografiya, 10(5), 635–643, 1965].

Manuscript received August 4, 1994
Manuscript accepted July 13, 1995